Action potentials drive body wall muscle contractions in *Caenorhabditis elegans*

Shangbang Gao[a] and Mei Zhen[a,b,c,1]

[a]Samuel Lunenfeld Research Institute, Mount Sinai Hospital, Toronto, ON, Canada M5G 1X5; and Departments of [b]Molecular Genetics, and [c]Physiology, University of Toronto, Toronto, ON, Canada M5S 1A8

Edited by Cornelia Bargmann, The Rockefeller University, New York, NY, and approved December 28, 2010 (received for review August 19, 2010)

The sinusoidal locomotion exhibited by *Caenorhabditis elegans* predicts a tight regulation of contractions and relaxations of its body wall muscles. Vertebrate skeletal muscle contractions are driven by voltage-gated sodium channel–dependent action potentials. How coordinated motor outputs are regulated in *C. elegans*, which does not have voltage-gated sodium channels, remains unknown. Here, we show that *C. elegans* body wall muscles fire all-or-none, calcium-dependent action potentials that are driven by the L-type voltage-gated calcium and Kv1 voltage-dependent potassium channels. We further demonstrate that the excitatory and inhibitory motoneuron activities regulate the frequency of action potentials to coordinate muscle contraction and relaxation, respectively. This study provides direct evidence for the dual-modulatory model of the *C. elegans* motor circuit; moreover, it reveals a mode of motor control in which muscle cells integrate graded inputs of the nervous system and respond with all-or-none electrical signals.

With the deciphering of the cell lineage (1) and the wiring diagram of the nervous system (2), *Caenorhabditis elegans* offers an attractive model to investigate fundamental mechanisms that govern neural development and communication (3, 4). However, its small size has long made it difficult to accommodate in situ electrophysiological studies. *C. elegans*' motor circuit, therefore, was initially modeled based on its anatomical analogy with *Ascaris*, large parasite nematodes that exhibit a similar sinusoidal locomotion pattern (2, 5). Electrophysiological analyses on *Ascaris* led to a dual-modulation model, where the somatic muscles receive both excitatory and inhibitory inputs to coordinate spatial–temporally correlated contractions (5–7). Anatomical studies in *C. elegans*, such as the electron microscopic reconstruction of the neuromuscular system (2), behavioral analyses followed by the ablation of specific neurons (8), and the identification of neurotransmitters and their receptors at neuromuscular junctions (9–11), lent strong support to a similar mechanism at its motor system. However, it was not until the development of *C. elegans* muscle preparations that the detection of cholinergic and GABAergic currents was allowed (12).

Questions remain as to how *C. elegans* encodes and transmits signals to control locomotion. Skeletal muscle contractions depend on excitation–contraction coupling, a process where muscle fibers fire action potentials in response to the excitatory inputs of the motor neurons and contract. Action potentials, the regenerative membrane depolarization events, are usually triggered by voltage-dependent sodium (Na^+) currents (13). *C. elegans* does not have voltage-gated Na^+ channels (12, 14). Indeed, most electrophysiological studies to date have alluded to a passive spread or to graded potentials in the nervous system, including motoneurons (14), whereas a few neurons exhibit plateau potentials with either an up or down excitation state through unknown mechanisms (15). *C. elegans* pharyngeal muscles fire spontaneous, cardiac-like action potentials that require both Na^+ and Ca^{2+} (16, 17). In body wall muscles, occasional spontaneous spike activities of varying amplitude were previously observed (18, 19), but current injections elicited only graded potentials (18). As most mature neuromuscular systems engage all-or-none action potentials for coordinated locomotion, how *C. elegans* locomotion is regulated remains unclear.

In this study, we performed whole-cell patch current-clamp recording with modified recording conditions and subsequently detected robust, all-or-none action potentials, both spontaneously and in response to depolarizing currents, by body wall muscles. We further dissect the channel components of these action potentials and demonstrate that (*i*) a single action potential by a muscle cell is sufficient to drive its contraction; (*ii*) excitatory motoneuron inputs potentiate action potential firing and muscle contractions; and (*iii*) inhibitory motoneuron activities block action potential firing, accompanied by muscle relaxation, providing a direct evidence for the dual-modulatory locomotion model.

Results

***C. elegans* Body Wall Muscles Fire Action Potentials.** How signals are coded and transmitted at the *C. elegans* motor circuit remains unclear. With modified intracellular recording conditions (*Materials and Methods*), we observed robust action potential–like spikes after the injection of either constant or ramp depolarizing currents in ~90% of preparations (Fig. 1 *A* and *B*). Trains of such signals were evoked by prolonged current injections (Fig. 1*C*). These signals fit all characteristics defining action potentials (20): they are all-or-none, constant in shape and amplitude, regardless of the level of supraliminal stimulus, and they are self-terminating and exhibit a stereotyped, biphasic waveform. Their peak amplitude and half-width time were 52.6 ± 1.8 mV and 15.5 ± 0.9 ms, respectively, which is smaller in amplitude but significantly longer in duration than those observed in mammalian skeletal muscles (21).

Spontaneous action potentials were also recorded in ~80% of preparations (Fig. 1*D*). The resting potential, −25.0 ± 1.0 mV (n = 27, Fig. 1*D*), was considerably more depolarized than that of the *C. elegans* pharyngeal (16) and vertebrate skeletal muscles (21). The high resting membrane potential probably resulted from a high chloride (Cl^-) permeability, as proposed for *Ascaris* muscles (22), instead of potassium (K^+) equilibrium (13).

There was no significant difference in either amplitude or kinetics between the evoked and spontaneous action potentials (Fig. 1*E*), and both were triggered at a threshold of approximately −10 mV (Fig. S1 *A* and *B*). In ~50% of our recordings, both low and high frequencies of spontaneous firing patterns were observed, resulting in an averaged spontaneous firing frequency of 0.73 ± 0.14 Hz (Fig. 1*D* and Table S1). Therefore, *C. elegans* body wall muscles are capable of firing action potentials in distinct patterns.

Body Wall Muscle Action Potentials Are Ca^{2+}-Driven. To determine the ion dependence of these action potentials, we examined the consequences of substituting Ca^{2+} or Na^+ in the extracellular solution on current injection–elicited action potentials. Action potential firing was abolished in the absence of Ca^{2+}, suggesting that Ca^{2+} is essential for initiating action potentials (Fig. 1*F*). No action potentials were elicited in the absence of Na^+ either;

Author contributions: S.G. and M.Z. designed research; S.G. performed research; S.G. contributed new reagents/analytic tools; S.G. and M.Z. analyzed data; and S.G. and M.Z. wrote the paper.

The authors declare no conflict of interest.

This article is a PNAS Direct Submission.

Freely available online through the PNAS open access option.

[1]To whom correspondence should be addressed. E-mail: zhen@lunenfeld.ca.

This article contains supporting information online at www.pnas.org/lookup/suppl/doi:10.1073/pnas.1012346108/-/DCSupplemental.

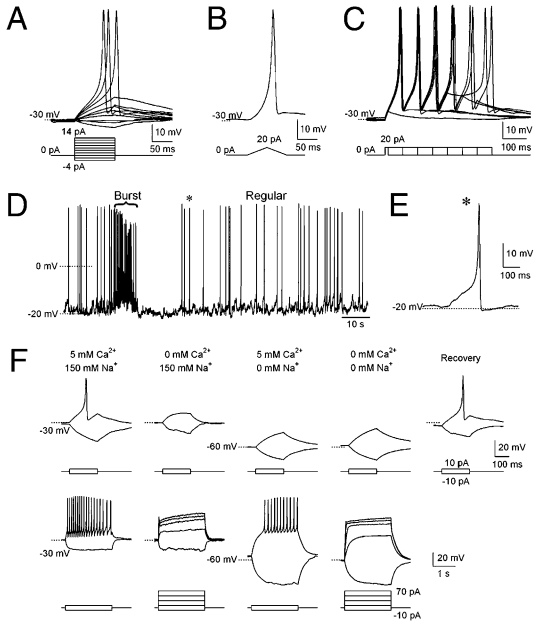

Fig. 1. *C. elegans* body wall muscles fire all-or-none action potentials. (*A*–*C*) Action potentials evoked by current steps from −4 to +14 pA in 2-pA increments (*A*), ramp currents from 0 to +20 pA (*B*), and +20 pA currents from 10- to 360-ms duration in 50-ms increments (*C*). Dotted lines, −30 mV. (*D*) Spontaneous action potentials exhibit "burst" (brace) and "regular" firing modes. (*E*) A scaled single spontaneous action potential labeled with asterisk *D*. (*F*) *Upper* traces show that single action potentials were abolished in the absence of Ca^{2+}, Na^{+}, or both. *Lower* traces show that, with increased current injection time and amplitude, trains of action potentials were elicited in normal and 0 Na^{+} solutions, but were not in 0 Ca^{2+}, or 0 Ca^{2+} and Na^{+} solutions.

moreover, the resting potential became hyperpolarized (−55.2 ± 2.4 mV), and the firing could be restored with increased current injection (3.0 ± 1.3 Hz) (Fig. 1*F*). When both Na^{+} and Ca^{2+} were removed, no action potentials were observed, and the resting potential also became hyperpolarized (−62.3 ± 5.4 mV). However, action potentials could no longer be restored by increased duration and amplitude of currents injected (Fig. 1*F*). These results suggest that Ca^{2+} plays a primary role in the initiation of action potentials, whereas Na^{+} affects action potential indirectly by maintaining the membrane potential.

L-Type Voltage-Gated Calcium Channel (VGCC) EGL-19 Elicits the Depolarization of Action Potentials. To identify the ion channels that elicit these action potentials, we compared the kinetics of spontaneous action potentials between wild-type (WT) and various channel mutants. *egl-19*, *unc-2*, and *cca-1* encode for the α1-subunit of the L-, R,N,P/Q-, and T-type VGCC, respectively (23–25). *unc-36* and *tag-180* encode the VGCC auxiliary $\alpha_2\delta$-subunits (4). *nca-1* and *nca-2* are components of a cation leak channel (26). Deletion, or severe loss-of-function (*lf*), alleles were examined in most cases. Because *egl-19* null animals are embryonically lethal, two viable, recessive, partial *lf* alleles, *n582* and *ad1006* (23), were examined.

Action potential frequency was severely reduced in both *egl-19 (lf)* mutants, as will be discussed in later sections. Remaining action potentials exhibited altered kinetics, with a significantly delayed onset and a prolonged duration in both alleles, as well as a reduced amplitude in *ad1006* (Fig. 2 *A* and *B* and Fig. S3). No change in action potential kinetics was observed in other mutants (Fig. S2*A*), suggesting that L-VGCC/EGL-19 is the main Ca^{2+} channel eliciting muscle action potentials. This is consistent with a previous finding that *egl-19(lf)* affects graded potentials in body wall muscles (18).

To further investigate how *egl-19(lf)* mutants affect action potential kinetics, we examined whole-cell Ca^{2+} currents in body wall muscles. Both *egl-19(lf)* mutants exhibited altered kinetics: in *n582*, the activation time constant showed a ∼10-fold increase (Fig. 3 *A* and *B*), similar to a previous report (18), whereas the deactivation time constants remained normal (Fig. 3*C*); *ad1006*, on the other hand, exhibited a normal activation time constant (Fig. 3 *A* and *B*) but abnormal deactivation kinetics, where the fast phase decay was absent (Fig. 3*C*). Both *egl-19* alleles exhibited a positive shift in the current–voltage curve (Fig. 3 *D* and *E*). The shift in the voltage dependence of activation, in combination with the altered kinetics of calcium currents in *egl-19* mutants, can account for the delay in the initiation and the broadening of action potentials. The peak current density was decreased by approximately threefold in *ad1006* but unaffected in *n582* (Fig. 3*F*), which is also consistent with a specific decrease of action potential amplitude in *ad1006* mutants.

The resting membrane potential of the body wall muscle was slightly elevated in *n582*, and unchanged in *ad1006* (Fig. 2*D*). Depolarized resting membrane potential likely contributes to a mildly increased threshold (Fig. S1*C*) and a slightly prolonged action potential firing (Fig. S4I). However, hyperpolarizing membrane potential did not restore the broadening of action potentials in *n582* (Fig. S4*B*). Together with the lack of obvious changes in *ad1006* (Fig. 2*D*), the depolarized resting membrane potential in *n582* was unlikely to account for the altered frequency and kinetics of action potentials in *egl-19(lf)* mutants. Together, these results support that L-VGCC/EGL-19 elicits action potentials in *C. elegans* body wall muscles.

Kv1 K^{+} Channel SHK-1 Affects the Repolarization of Action Potentials. The termination of action potentials requires voltage-gated K^{+} (termed "Kv") channels. The *C. elegans* genome predicts >70 K^{+} channel components (4). Three of these, *shk-1*, *shl-1*, and *slo-2*,

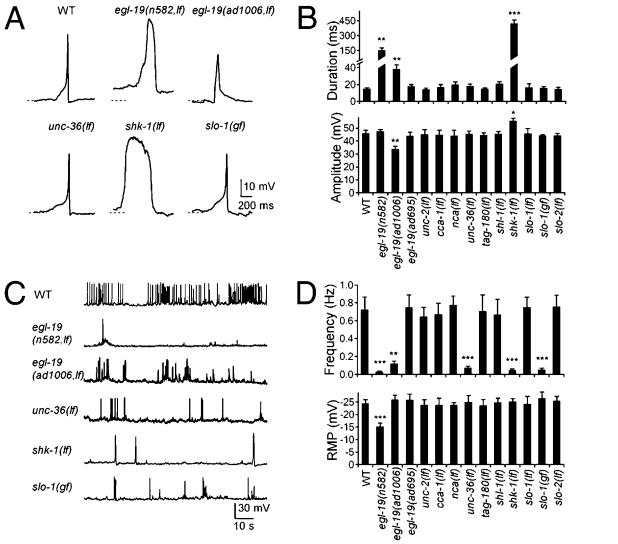

Fig. 2. Channels responsible for action potentials in *C. elegans* body wall muscles. (*A*) Representative single action potentials from WT and channel mutant muscles. Pronounced changes in kinetics were present in *egl-19(n582, lf)*, *egl-19(ad1006,lf)*, and *shk-1(lf)* but absent from *unc-36(lf)* and *slo-1(gf)* mutants. Dashed lines, −20 mV. (*B*) Quantification of the half-width and peak amplitude of action potentials in the respective channel mutants. An extension of duration was observed in *egl-19(n582,lf)*, *egl-19(ad1006,lf)*, and *shk-1(lf)*. There was an increase of the peak amplitude in *shk-1(lf)* mutants but a decrease in *egl-19(ad1006,lf)* mutants. (*C*) Representative traces for trains of spontaneous action potentials in WT and mutant animals. (*D Upper*) The frequency of action potentials was decreased in *egl-19(n582,lf)*, *egl-19(ad1006,lf)*, *unc-36(lf)*, *shk-1 (lf)*, and *slo-1(gf)* mutants. (*Lower*) The resting membrane potential was elevated in *egl-19(n582,lf)* mutants. **P* < 0.05; ***P* < 0.01; ****P* < 0.001; *t* test against WT. (Error bars = SEM.)

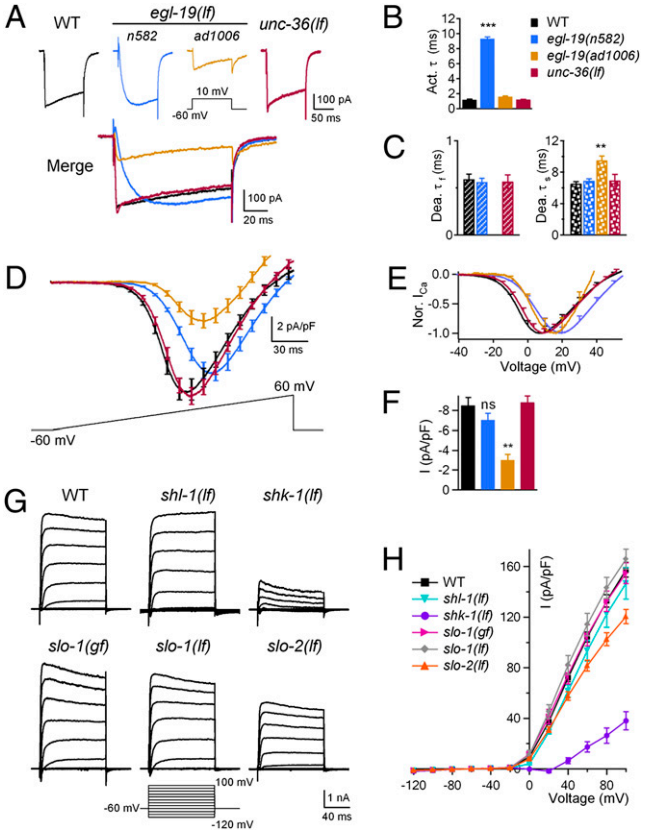

Fig. 3. *lf* mutations in L-VGCC/EGL-19 and Kv1/SHK-1 affect the voltage-dependent Ca^{2+} and K^+ currents. (*A*) Representative voltage-gated Ca^{2+} currents of WT, *egl-19(n582,lf)*, *egl-19(ad1006,lf)*, and *unc-36(lf)* mutants. (*B*) Ca^{2+} current activation time constants (activation τ) were increased in *egl-19(n582,lf)* mutants. (*C*) The fast (Dea. τ_f) component of Ca^{2+} current deactivation time constants was abolished, and the slow (Dea. τ_s) component was delayed in *egl-19(ad1006,lf)* mutants. (*D*) Current–voltage (*I–V*) relationship of VGCC was affected in *egl-19(n582,lf)* and *egl-19(ad1006,lf)* but not *unc-36(lf)*. (*E*) Normalized *I–V* curve showed that the voltage dependence was shifted by approximately +10 mV in *egl-19(n582,lf)* and by approximately +5 mV in *egl-19(ad1006,lf)*. (*F*) The peak Ca^{2+} current density was decreased approximately threefold in *egl-19(ad1006,lf)* animals but unaffected in *egl-19(n582,lf)* and *unc-36(lf)* mutants. (*G* and *H*) K^+ current densities showed a significant decrease in *shk-1(lf)* and a slight reduction in *slo-2(lf)* mutants at ≥+40 mV. ns, not significant; $^{**}P < 0.01$; $^{***}P < 0.001$; *t* test against WT. (Error bars: SEM.)

were reported to be expressed in both body wall muscles and neurons, and they constitute the macroscopic outward K^+ currents in cultured muscle cells (27–29). SHK-1 and SHL-1 are α-subunits of the Kv1 and Kv4 voltage-gated K^+ channels, respectively, whereas *slo-2* encodes a subunit of a Na^+ and Cl^- activated K^+ (K_{Na}) channel (27). SLO-1, the BK-type K^+ channel, is also expressed in both body wall muscles and neurons (30, 31).

Among these mutants, only *Kv1/shk-1(lf)* affected action potential firing (Fig. 2 *A* and *B* and Fig. S3). In addition to a drastic reduction of action potential frequency (discussed in later sections), the remaining action potentials in *Kv1/shk-1(lf)* exhibited a >30-fold increase in duration and a moderately increased amplitude (Table S1), suggesting that Kv1/SHK-1 affects the action potential termination. We further examined the contribution of Kv1/SHK-1 in voltage-gated K^+ currents in muscles. These currents were significantly reduced in *kv1/shk-1(lf)* but were minimally affected in other mutants (Fig. 3 *G* and *H*), consistent with Kv1/SHK-1 being a key voltage-gated K^+ channel involved in the repolarization of action potentials under our experimental conditions.

Voltage-Dependent Ca^{2+} and K^+ Channels Regulate Action Potential Frequency. Among the mutants examined, *L-VGCC/egl-19(lf)* and *Kv1/shk-1(lf)*, *$\alpha_2\delta$/unc-36(lf)*, and *BK/slo-1(gf)* animals exhibited a reduced frequency of spontaneous action potentials (Fig. 2 *C* and *D* and Fig. S2*B*). Unlike the case for *L-VGCC/egl-19(lf)* and *Kv1/shk-1(lf)*, no difference in the action potential kinetics, or voltage-dependence of Ca^{2+} or K^+ currents in muscles, was observed for *$\alpha_2\delta$/unc-36(lf)* (Fig. 3 *A–F*) or *BK/slo-1(gf)* (Fig. 3 *G* and *H*). UNC-36 and SLO-1 therefore likely affect muscle excitability indirectly. Given their broad neuronal expression, this result may reflect an effect of altered motoneuron inputs.

The defects of *egl-19(lf)* and *shk-1(lf)* are more complex because both mutants exhibit altered action potential kinetics (Fig. 2 *A* and *B*) as well as decreased action potential frequency (Fig. 2 *C* and *D*). As L-VGCC/EGL-19 and Kv1/SHK-1 channels are present in both neurons and muscles (23, 29), they may affect action potential frequency independently by modulating motoneuron inputs. Alternatively, the decreased spontaneous firing may reflect altered muscle cell membrane properties caused by altered action potential kinetics.

To distinguish between these possibilities, we compared the kinetics and frequency of spontaneous action potentials in *egl-19 (n582)* mutants that carried a functional *EGL-19* transgene in different tissues by mosaic analyses and tissue-specific rescue. When the transgene was present in both neurons and muscles, the frequency and duration of the action potentials were fully restored (Fig. 4 *A–C*). When the transgene was present in neurons alone, only the frequency of action potentials was rescued (Fig. 4 *A–C*), suggesting that frequency was strictly regulated through a neuronal role of L-VGCC/EGL-19. During this analysis, we did not obtain a sufficient number of muscle-specific mosaic animals. We used an alternative strategy where we expressed *EGL-19* minigene by a body wall muscle–specific promoter in *egl-19(n582)* mutants. In these animals, the resting membrane potential was fully restored (Fig. 4 *A* and *D*), and the duration of action potential was partially restored, whereas the frequency remained reduced (Fig. 4 *A–C*).

Together, these results indicate that L-VGCC/EGL-19, and probably also Kv1/SHK-1, have dual functions, where they participate in the initiation and termination of action potentials in body wall muscles and independently modulate the frequency of action potential firing through their effects on neural activities.

Motoneurons Regulate Action Potential Firing in Body Wall Muscles. To investigate whether muscle excitability is regulated by neuronal inputs, we first examined a severe *lf* allele for UNC-13, a conserved presynaptic protein required for synaptic transmission (32). *unc-13(lf)* mutants showed a severe reduction in the action potential frequency (0.04 ± 0.01 Hz), whereas, as expected, the resting potential and the kinetics of the remaining action potentials were normal (Fig. 4 *E* and *F*).

C. elegans body wall muscles receive both excitatory (cholinergic) and inhibitory (GABAergic) motoneuron inputs. To isolate the effect of excitatory inputs, we blocked acetylcholine (ACh) receptors with D-tubocurarine (dTBC) in *zxIs6* animals. These animals express a light-gated cation channel, channelrhodopsin-2 (ChR2) in cholinergic neurons (33), allowing excitatory neuromuscular junctions to be specifically activated by light stimulation (34). As reported (34), the application of 0.5 mM dTBC resulted in a ~96% blockage of the ACh receptor currents evoked by a 10-ms light stimulation, and this effect was reversible upon washout (Fig. 4 *G* and *H*). Spontaneous action potentials were also reversibly blocked by ~88% (Fig. 4 *I* and *J*). Thus, cholinergic synaptic transmission is critical for potentiating action potential firing in body wall muscles. The application of 0.5 mM GABA, on the other hand, completely blocked the firing of action potentials (Fig. 4 *K* and *L*), consistent with GABAergic synaptic transmission inhibiting action potentials in body wall muscles.

A Single Action Potential Is Sufficient to Drive Muscle Contraction. To explore the physiological relevance of these action potentials, we induced action potentials in *zxIs6* animals by light stimulation and simultaneously recorded the muscle response. Each single action

NEUROSCIENCE

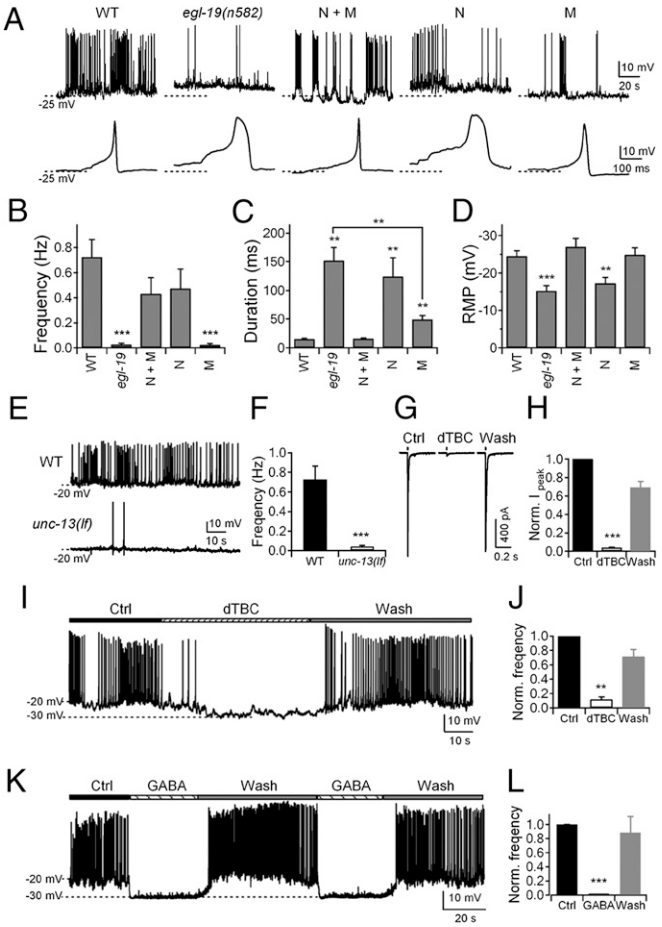

Fig. 4. Neuronal activity modulates spontaneous action potential frequency in body wall muscles. (*A*–*D*) Neuronal L-VGCC/EGL-19 modulates the frequency of action potentials, whereas muscle EGL-19 initiates action potentials. (*A Upper*) Single and trains of action potentials in WT, *egl-19(n582)*, and *egl-19(n582)* animals expressing EGL-19 in neurons and muscles (N + M, $n = 6$), neurons (N, $n = 3$), and muscles (M, $n = 5$). (*B*) Action potential frequency was rescued in N + M and N, but not in M. (*C*) The duration of action potentials was rescued in N + M and partially rescued in M, but not in N. (*D*) The resting membrane potential was rescued in N + M and M, but not in N. (*E* and *F*) Spontaneous action potential frequency was reduced in *unc-13(lf)* mutants ($n = 7$) compared with WT ($n = 10$). (*G*) Representative traces of action potential firing in *zxIs6* animals when activated by 10-ms light stimulation, treated with 0.5 mM dTBC. (*H*) Quantification of ACh receptor currents during and after dTBC treatment ($n = 9$). (*I* and *J*) Frequency of action potential firing during dTBC treatment ($n = 7$). (*K* and *L*) Complete and reversible inhibition of action potential firing upon 0.5 mM GABA treatment ($n = 6$). $^{**}P < 0.01$; $^{***}P < 0.001$; *t* test against WT or control. (Error bars: SEM.)

potential, evoked by 1-ms light stimulation, elicited a brief muscle contraction (Fig. 5 *A* and *B* and Movie S2). A 1-s stimulation induced a train of action potentials (~13 Hz), accompanied by a sustained tonic muscle contraction (Fig. 5 *A* and *B* and Movie S3). By contrast, no contraction was observed upon a 0.1-ms light pulse that triggered only a subthreshold voltage response (Fig. 5 *A* and *B* and Movie S1). Muscle contractions were also tightly correlated with single action potential firings in *egl-19(n582)* animals (Fig. S5 and Movie S4), further supporting that these muscle contractions are activated by action potentials, not caused by photostimulation-induced artifacts. Therefore, not only do these action potentials correspond to muscle activities, but also a single action potential is sufficient to drive muscle contraction.

GABAergic Inputs Prevent Action Potential and Lead to Muscle Relaxation. It has long been speculated that the inhibitory GABAergic synaptic transmission underlies contralateral muscle relaxation, contributing to the sinusoidal locomotion pattern (2). Consistently, the application of GABA to body wall muscles blocked the firing of action potentials (Fig. 4 *K* and *L*). We further investigated whether GABAergic motoneuron activity inhibits action potential firing in body wall muscles. Applying light stimulation to *zxIs3* animals that expressed ChR2 in GABAergic motoneurons (34), we simultaneously recorded the electrical and mechanical activities of body wall muscles. The spontaneous action potentials were completely blocked when GABA release was triggered (Fig. 5*C*). The inhibition was instant and reversible after the stimulation was removed (Fig. 5*C*). The inhibition likely resulted from a GABA receptor–dependent resting potential hyperpolarization: upon stimulation, the resting membrane potential was decreased (Fig. 5*C*), bringing it close to the reversal potential of the ionotropic GABA receptor (Fig. S6). This hyperpolarization was accompanied by the relaxation of body wall muscles (Fig. 5*D* and Movie S5), providing the direct evidence that GABAergic inputs lead to the muscle relaxation (34).

Body Wall Muscle Action Potentials Correlate with Locomotion. With the exception of *shk-1(lf)*, all mutants with altered action potential patterns, *egl-19(lf)*, *unc-36(lf)*, and *slo-1(gf)*, also exhibited sluggish locomotion, quantified as reduced body-bending in liquid (Fig. S7*A*). Although *shk-1(lf)* showed normal locomotion, *shk-1(lf);egl-19(lf)* mutants exhibited further reduced locomotory

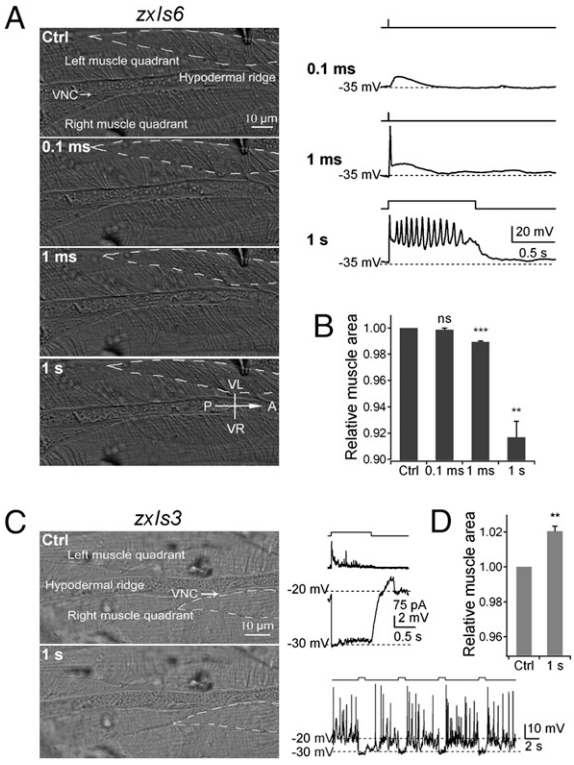

Fig. 5. Action potentials drive body wall muscle contractions. (*A Left*) Representative muscle morphology before and after 0.1-ms, 1-ms, and 1-s light stimulation. VNC, ventral neural cord. (*Right*) The membrane potential in response to light stimulation in the same muscle. (*B*) Normalized muscle surface cell areas outlined by dashed lines in *A*. (*C*) In *zxIs3* animals, GABAergic motoneurons hyperpolarize and drive relaxation. (*Left*) Representative muscle morphologies before and after 1-s light stimulation. (*Right*) Changes in membrane potential of body muscle cells during light stimulation. Four consecutive 1-s light stimulations induced muscle hyperpolarization and completely inhibited spontaneous action potential firing (*Lower Right*). (*D*) This inhibition correlated with muscle relaxation, shown by increased cell areas ($n = 4$). ns, not significant; $^{**}P < 0.01$; $^{***}P < 0.001$; *t* test against control. (Error bars: SEM.)

activity and more severe paralysis than *egl-19(lf)* alone (Fig. S7*A*). These data support that the ability of body wall muscles to fire action potentials correlates with locomotion.

To further examine whether a defective locomotion in *egl-19 (n582)* mutants is caused by reduced frequency of muscle spiking, and/or defective spiking kinetics, we examined the motor activity, both in liquid (Fig. S7*B*) and on plates (Fig. S7 *C* and *D*), of *egl-19(n582)* animals expressing the functional *EGL-19* transgene in either neurons or muscles. Reduced locomotion of *egl-19(n582)* was partially restored by neuronal *EGL-19* transgene, but was either unaffected (in liquid, Fig. S7*B*) or very slightly improved by muscle *EGL-19* transgene (on plate, Fig. S7 *C* and *D*). Because the neuronal *EGL-19* transgene specifically restored the frequency of muscle spiking (Fig. 4*B*), and the muscle *EGL-19* only rescued the kinetics of spiking in *egl-19 (n582)* animals (Fig. 4*C*), these results imply that infrequent firing of action potentials, rather than the defective action potential kinetics of muscle cells contributes more significantly to reduced locomotion of *egl-19(n582)* animals. However, locomotion was only fully rescued when *EGL-19* transgene was present in both neurons and muscles (Fig. S7 *B* and *C*), coinciding with muscle cells exhibiting both high spiking frequency and proper spiking kinetics (Fig. 4 *B* and *C*). Therefore, rescued action potential kinetics did contribute to locomotion in *egl-19 (n582)* transgenic animals, albeit in a minor manner that was more difficult to detect by behavioral assays.

An All-or-None Output of the *C. elegans* Body Wall Muscles. A recent study implied that motoneurons transmit signals in a graded fashion (35). To test whether this is the case with our recording conditions, we stimulated cholinergic motoneurons in *zxIs6* with 1-ms light pulses of different light intensity and recorded both the resulting postsynaptic currents (in voltage-clamp mode) and membrane potentials (in current-clamp mode) in muscles (Fig. 6*A*). Although the amplitude of the postsynaptic receptor ion influx correlated with the light intensity, these currents triggered all-or-none action potentials identical to those we described earlier (Fig. 6 *A* and *B*). On average, a postsynaptic current of -67.9 ± 7.5 pA was required to trigger a single action potential (Fig. 6*C*). More action potentials were triggered with both increased light stimulation and postsynaptic currents (Fig. 6 *A* and *C*).

Together, these studies support the following model: through the ability to fire and alter the frequency of Ca^{2+}-dependent action potentials in response to excitatory and inhibitory motoneuron inputs, *C. elegans* body wall muscles integrate graded neuronal inputs and use all-or-none electrical signals to coordinate muscle contraction and relaxation, as well as to drive locomotion (Fig. 6*D*).

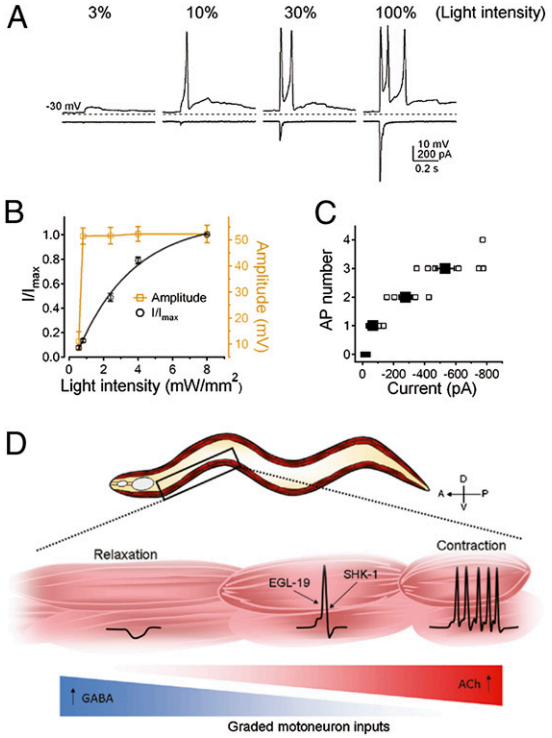

Fig. 6. Action potential-driven muscle contraction and relaxation in response to graded motoneuron inputs. (*A*) Graded postsynaptic currents (at −30 mV) evoked all-or-none action potentials (at 0 pA). 3%, 10%, 30%, and 100% indicate the percentage of the full light stimulation. Dashed lines, −30 mV. Data were recorded from the same muscle cell every 30 s. (*B*) Normalized postsynaptic currents (○, $n = 14$) and corresponding membrane potential peak amplitude (□, $n = 11$) were plotted against light intensity. The normalized postsynaptic currents were fitted with a single exponential function. (*C*) The number of action potentials plotted against the amplitude of postsynaptic currents ($n = 8$). (Error bars = SEM.) (*D*) Graphical representation of a model: In response to graded motoneuron inputs, muscle cells fire action potentials that coordinate the contraction or relaxation along the body.

Discussion

***C. elegans* Body Wall Muscles Fire Action Potentials.** In this study, we detected spontaneous and stimulus-induced all-or-none action potentials in *C. elegans* body wall muscles. We used the standard dissection and whole-cell patch-clamp techniques but reduced the Cl^- concentration in the intracellular recording solution. High Cl^- content in the original formula may have activated Cl^--activated K^+ channels (27, 28) and inhibited frequent action potential firing. Such a modified condition appears more suitable to examine the physiological properties of *C. elegans* neuromuscular junctions because the Cl^- reversal potential, approximately −30 mV, corresponds to an inhibitory property of the ionotropic GABA receptor at body wall muscles, which exhibit a resting potential of approximately −25 mV under this recording condition.

The spontaneous spiking activity in body wall muscles was observed previously (18, 19). However, unlike the all-or-none signals, the spike amplitude was variable, and current injection induced graded potentials. These graded potentials were also affected by L-VGCC/EGL-19 (18). We speculate that both studies detected similar electrical properties of the body wall muscle, but these signals are more stable under the recording and dissection conditions implemented in this study. Together with the strong correlations we observed between these action potentials and muscle contraction or relaxation, these electrical signals likely correlate with the physiological activities of the *C. elegans* neuromuscular system.

These action potentials exhibit distinct features: they are purely Ca^{2+} driven, the peak amplitude is significantly smaller compared with action potentials of the *C. elegans* pharyngeal (17) and vertebrate skeletal muscles (21), and their duration was approximately eightfold longer than those of vertebrate skeletal muscles. These findings are consistent with depolarization being driven by L-VGCCs instead of the fast-inactivating Na^+ channels. Single or trains of spontaneous Ca^{2+}-driven action potentials have been observed in *Ascaris* muscle cells (36, 37). However, they were with a more variable, 10- to 50-ms duration and a smaller peak amplitude up to ∼30 mV (37). *Ascaris* muscle cells exhibited several other spontaneous electrical activity patterns; for example, the short or long membrane potential oscillations consisted of spikes with considerable fluctuations of peak amplitudes (37), which were never observed in our preparations. The distinct patterns of electrical activities for *Ascaris* muscles probably reflect the difference in the locomotion pattern between the large, parasite and small, free-living nematodes and/or in the experimental conditions.

L-VGCC Elicits Action Potentials in Body Wall Muscles. L-VGCC/EGL-19 is the main Ca^{2+} channel eliciting action potentials in *C. elegans* body wall muscles, whereas, in the pharyngeal muscles,

both L- and T-type VGCCs contribute to shape action potentials with an extended plateau depolarization phase (25). Although these action potentials are Ca^{2+}-driven, their firing, nevertheless, also critically depends on Na^+. A Na^+ dependence of excitability, which was attributed to the Na^+ conductance through other channels such as VGCCs (16), was also observed in *C. elegans* pharyngeal muscles. In body wall muscles, however, the Na^+ dependence is because of its role in establishing the resting membrane potential, an effect that may involve a Na^+ pump (17).

Interestingly, most invertebrates also rely on Ca^{2+} channels for muscle excitation and contraction. Although vertebrate muscles generate Na^+-dependent action potentials to initiate their excitation, L-type Ca^{2+} channels are involved in excitation–contraction coupling. Therefore, the role of L-VGCC in the *C. elegans* motor system may represent an evolutionarily conserved mechanism for body wall muscle excitation that became further refined in the vertebrate neuromuscular system.

Kv1 and Other Unidentified K^+ Channels Terminate Action Potentials. Although Kv1, Kv4, and K_{Na} all contributed to the voltage-dependent K^+ currents in cultured muscle cells (28, 29), our analyses of the respective deletion mutants only identified a significant reduction of voltage-evoked K^+ currents in *Kv1/shk-1* animals. Consistently, *Kv1/shk-1* alone affected action potential repolarization, supporting a conserved role of the Kv1 in action potential termination. As membrane repolarization eventually occurred in *Kv1/shk-1* deletion mutants, other K^+ channels were activated to terminate action potentials under our experimental conditions. We speculate that other functionally redundant, voltage- or Ca^{2+}-activated K^+ channels are involved in the termination of action potentials, which would account for the lack of obvious locomotion defect in *kv1/shk-1* single mutants, whereas it enhanced the locomotory defects of another action potential–defective mutant *egl-19*. Identities of additional K^+ channels that are involved in action potential firing are unknown.

Dual Neural Modulation Underlies Coordinated Locomotion. Under such recording conditions, the resting potential of body wall muscles (approximately −25 mV) resides between the reversal potentials of ACh (+20 mV) and GABA (−30 mV) receptors (Fig. S6), allowing its excitability to be increased by ACh and decreased by GABA. Such a membrane property is perfectly suited for the proposed dual-modulatory model of the *C. elegans* motor circuit. Indeed, cholinergic motoneuron activity led to an increase of action potential frequency, whereas an activation of GABAergic motoneurons hyperpolarized the membrane and prevented action potential firing in muscle cells. Moreover, the potentiation or inhibition of action potentials directly correlated with muscle contraction or relaxation, respectively.

In summary, we show that action potentials, driven by voltage-gated Ca^{2+} and K^+ channels and regulated by both excitatory and inhibitory motoneuron activities, underlie *C. elegans* body wall muscle contraction and relaxation. This study not only provides the direct experimental evidence for the dual-innervation model for the *C. elegans* motor circuit, but it also further implies that its body wall muscles can integrate graded neuronal inputs and deliver all-or-none electrical outputs to drive locomotion.

Materials and Methods

Electrophysiology. The pipette solution contained (in mM): 115 K-gluconate; 25 KCl; 0.1 $CaCl_2$; 5 $MgCl_2$; 1 BAPTA; 10 Hepes; 5 Na_2ATP; 0.5 Na_2GTP; 0.5 cAMP; 0.5 cGMP, pH 7.2, with ~320 mosM KOH. The extracellular solution contained (in mM): 150 NaCl; 5 KCl; 5 $CaCl_2$; 1 $MgCl_2$; 10 glucose; 5 sucrose; 15 Hepes, pH 7.3, with ~330 mosM NaOH.

Methods for other experiments are provided in *SI Materials and Methods*.

ACKNOWLEDGMENTS. We thank Y. Wang, H. Li, and T. Kawano for technical support; C. Bargmann, J. Richmond, M. Bouhours, J. Georgiou, and C. Hwang for comments and input; and the *Caenorhabditis* Genetics Center and A. Gottschalk for strains. This work is supported by the Canadian Institutes of Health Research (M.Z).

1. Sulston JE, Schierenberg E, White JG, Thomson JN (1983) The embryonic cell lineage of the nematode *Caenorhabditis elegans*. *Dev Biol* 100:64–119.
2. White JG, Southgate E, Thomson JN, Brenner S (1986) The structure of the nervous system of the nematode *Caenorhabditis elegans*. *Philos Trans R Soc Lond B Biol Sci* 314:1–340.
3. Brenner S (1974) The genetics of *Caenorhabditis elegans*. *Genetics* 77:71–94.
4. Bargmann CI (1998) Neurobiology of the *Caenorhabditis elegans* genome. *Science* 282:2028–2033.
5. Davis RE, Stretton AO (1989) Passive membrane properties of motorneurons and their role in long-distance signaling in the nematode *Ascaris*. *J Neurosci* 9:403–414.
6. Walrond JP, Stretton AO (1985) Excitatory and inhibitory activity in the dorsal musculature of the nematode *Ascaris* evoked by single dorsal excitatory motonerons. *J Neurosci* 5:16–22.
7. Walrond JP, Kass IS, Stretton AO, Donmoyer JE (1985) Identification of excitatory and inhibitory motoneurons in the nematode *Ascaris* by electrophysiological techniques. *J Neurosci* 5:1–8.
8. Chalfie M, et al. (1985) The neural circuit for touch sensitivity in *Caenorhabditis elegans*. *J Neurosci* 5:956–964.
9. McIntire SL, Jorgensen E, Horvitz HR (1993) Genes required for GABA function in *Caenorhabditis elegans*. *Nature* 364:334–337.
10. Alfonso A, Grundahl K, Duerr JS, Han HP, Rand JB (1993) The *Caenorhabditis elegans* unc-17 gene: A putative vesicular acetylcholine transporter. *Science* 261:617–619.
11. Jin Y, Jorgensen E, Hartwieg E, Horvitz HR (1999) The *Caenorhabditis elegans* gene *unc-25* encodes glutamic acid decarboxylase and is required for synaptic transmission but not synaptic development. *J Neurosci* 19:539–548.
12. Richmond JE, Jorgensen EM (1999) One GABA and two acetylcholine receptors function at the *C. elegans* neuromuscular junction. *Nat Neurosci* 2:791–797.
13. Hille B (2001) *Ion Channels of Excitable Membranes* (Sinauer, Sunderland, MA), 3rd Ed.
14. Goodman MB, Hall DH, Avery L, Lockery SR (1998) Active currents regulate sensitivity and dynamic range in *C. elegans* neurons. *Neuron* 20:763–772.
15. Mellem JE, Brockie PJ, Madsen DM, Maricq AV (2008) Action potentials contribute to neuronal signaling in *C. elegans*. *Nat Neurosci* 11:865–867.
16. Franks CJ, et al. (2002) Ionic basis of the resting membrane potential and action potential in the pharyngeal muscle of *Caenorhabditis elegans*. *J Neurophysiol* 87: 954–961.
17. Davis MW, et al. (1995) Mutations in the *Caenorhabditis elegans* Na,K-ATPase α-subunit gene, *eat-6*, disrupt excitable cell function. *J Neurosci* 15:8408–8418.
18. Jospin M, Jacquemond V, Mariol MC, Ségalat L, Allard B (2002) The L-type voltage-dependent Ca^{2+} channel EGL-19 controls body wall muscle function in *Caenorhabditis elegans*. *J Cell Biol* 159:337–348.
19. Jospin M, Allard B (2004) An amiloride-sensitive H^+-gated Na^+ channel in *Caenorhabditis elegans* body wall muscle cells. *J Physiol* 559:715–720.
20. Hodgkin AL, Huxley AF (1952) A quantitative description of membrane current and its application to conduction and excitation in nerve. *J Physiol* 117:500–544.
21. Keynes RD, Aidley DJ (2001) *Nerve and Muscle* (Cambridge Univ Press, Cambridge, UK).
22. Brading AF, Caldwell PC (1971) The resting membrane potential of the somatic muscle cells of *Ascaris* lumbricoides. *J Physiol* 217:605–624.
23. Lee RY, Lobel L, Hengartner M, Horvitz HR, Avery L (1997) Mutations in the α1 subunit of an L-type voltage-activated Ca^{2+} channel cause myotonia in *Caenorhabditis elegans*. *EMBO J* 16:6066–6076.
24. Schafer WR, Kenyon CJ (1995) A calcium-channel homologue required for adaptation to dopamine and serotonin in *Caenorhabditis elegans*. *Nature* 375:73–78.
25. Shtonda B, Avery L (2005) CCA-1, EGL-19 and EXP-2 currents shape action potentials in the *Caenorhabditis elegans* pharynx. *J Exp Biol* 208:2177–2190.
26. Yeh E, et al. (2008) A putative cation channel, NCA-1, and a novel protein, UNC-80, transmit neuronal activity in *C. elegans*. *PLoS Biol* 6:e55.
27. Yuan A, et al. (2000) SLO-2, a K^+ channel with an unusual Cl^- dependence. *Nat Neurosci* 3:771–779.
28. Santi CM, et al. (2003) Dissection of K^+ currents in *Caenorhabditis elegans* muscle cells by genetics and RNA interference. *Proc Natl Acad Sci USA* 100:14391–14396.
29. Fawcett GL, et al. (2006) Mutant analysis of the Shal (Kv4) voltage-gated fast transient K^+ channel in *Caenorhabditis elegans*. *J Biol Chem* 281:30725–30735.
30. Wang ZW, Saifee O, Nonet ML, Salkoff L (2001) SLO-1 potassium channels control quantal content of neurotransmitter release at the *C. elegans* neuromuscular junction. *Neuron* 32:867–881.
31. Liu Q, Chen B, Ge Q, Wang ZW (2007) Presynaptic Ca^{2+}/calmodulin-dependent protein kinase II modulates neurotransmitter release by activating BK channels at *Caenorhabditis elegans* neuromuscular junction. *J Neurosci* 27:10404–10413.
32. Richmond JE, Davis WS, Jorgensen EM (1999) UNC-13 is required for synaptic vesicle fusion in *C. elegans*. *Nat Neurosci* 2:959–964.
33. Nagel G, et al. (2003) Channelrhodopsin-2, a directly light-gated cation-selective membrane channel. *Proc Natl Acad Sci USA* 100:13940–13945.
34. Liewald JF, et al. (2008) Optogenetic analysis of synaptic function. *Nat Methods* 5: 895–902.
35. Liu Q, Hollopeter G, Jorgensen EM (2009) Graded synaptic transmission at the *Caenorhabditis elegans* neuromuscular junction. *Proc Natl Acad Sci USA* 106:10823–10828.
36. Del Castillo J, De Mello WC, Morales T (1967) The initiation of action potentials in the somatic musculature of *Ascaris* lumbricoides. *J Exp Biol* 46:263–279.
37. Weisblat DA, et al. (1976) Ionic mechanisms of electrical activity in somatic muscle of the nematode *Ascaris* lumbricoides. *J Comp Physiol* 111:93–113.

Supporting Information

Gao and Zhen 10.1073/pnas.1012346108

SI Materials and Methods

Strains and Culturing Conditions. The following strains were used in this study: N2 Bristol as WT, MT1212 *egl-19(n582) IV*, DA1006 *egl-19(ad1006) IV*, DA695 *egl-19(ad695) IV*, CB55 *unc-2(e55) X*, JD21 *cca-1(ad1650) X*, ZM1659 *nca-2(gk5) X;nca-1(gk9) IV*, CB251 *unc-36(e251) III*, VC550 *tag-180(ok779) II*, RB1144 *shl-1 (ok1168) IV*, RB1392 *shk-1(ok1581) II*, NM1968 *slo-1(js379lf) V*, CX3933 *slo-1(ky389) V*, LY100 *slo-2(nf100) X*, CB1091 *unc-13 (e1091) I*, ZX460 *zxIs6* [*Punc-17::ChR2(H134R)::YFP; lin-15*$^+$] *IV*, and ZX426 *zxIs3* [*Punc-47::ChR2(H134R)::YFP; lin-15*$^+$]. All strains were outcrossed against N2 at least twice. All strains were obtained from the *Caenorhabditis* Genetics Center (University of Minnesota, Minneapolis, MN) with the exception of *zxIs6* and *zxIs3*, which were received from A. Gottschalk (Goethe University, Frankfurt, Germany). All strains were cultured at 22 °C on nematode growth medium (NGM) plates seeded with OP50 unless specified otherwise (1). *zxIs6* and *zxIs3* were cultured in the dark at 22 °C on OP50-seeded NGM plates supplemented with *all-trans* retinal as described previously (2).

Electrophysiology. Recordings from dissected *C. elegans* body wall muscles were performed as described previously (3) but with modified recording solutions (see below). Briefly, 1-d-old hermaphrodite adults were glued to slides, and the body wall muscles were exposed by lateral excisions. The integrity of the anterior ventral body muscle and the ventral nerve cord were visually examined via differential interference contrast microscopy, and muscle cells were patched with fire-polished 4- to 6-MΩ resistant borosilicate pipettes (World Precision Instruments). Membrane currents and membrane potentials were recorded in the whole-cell configuration by a Digi-Data 1440A and a MultiClamp 700A amplifier using the Clampex 10 software, and data were processed with Clampfit 10 (Molecular Devices). Data were digitized at 10–20 kHz and filtered at 2.6 kHz. Cell resistance and capacitance were determined with Clampex (Molecular Devices) by applying a 10-mV depolarizing pulse with a holding potential of −60 mV, which was used to calculate the density of Ca^{2+} and K^+ currents (pA/pF). Leak currents were not subtracted.

Light stimulation of *zxIs6* and *zxIs3* was performed with an LED lamp (KSL-70; RAPP OptoElectronic) at a wavelength of 470 nm (8 mW/mm^2), controlled by the Axon amplifier software. Videos were recorded with a CCD digital camera (Zeiss Axiocam or Hamamatsu C2400) at 200 ms per frame. Simultaneous recordings of the muscle contraction and spiking activity were performed. Solution exchange was driven by gravity and completed in 5 s. All experiments were performed at room temperatures (20–22 °C).

Recording Solutions. For recording membrane potentials and K^+ currents, the pipette solution contained (in mM): 115 K-gluconate; 25 KCl; 0.1 $CaCl_2$; 5 $MgCl_2$; 1 BAPTA; 10 Hepes; 5 Na_2ATP; 0.5 Na_2GTP; 0.5 cAMP; 0.5 cGMP, pH 7.2, with~320 mosM KOH. cAMP and cGMP were included to maintain the activity and longevity of the preparation. The extracellular solution consisted of (in mM): 150 NaCl; 5 KCl; 5 $CaCl_2$; 1 $MgCl_2$; 10 glucose; 5 sucrose; 15 Hepes, pH 7.3 with ~330 mosM NaOH. For 0 Ca^{2+} extracellular solution, $CaCl_2$ was substituted with 5 mM $MgCl_2$ and 1 mM EGTA. For 0 Na^+ solutions, external Na^+ was replaced with the large cation *N*-methyl-D-glucamine ($NMDG^+$) or $Tris^+$. For recording voltage-dependent Ca^{2+} currents, the pipette solution contained (in mM): 140 CsCl; 10 TEA-Cl; 5 $MgCl_2$; 5 EGTA; 10 Hepes, pH 7.2, with ~320 mosM CsOH. The extracellular solution contained (in mM): 140 TEA-Cl; 5 $CaCl_2$; 1 $MgCl_2$; 3 4-aminopyridine ; 10 glucose; 5 sucrose; 15 Hepes, pH 7.4, with ~330 mosM CsOH. Chemical regents and blockers were obtained from Sigma unless stated otherwise.

Thrashing Assay for Body Bends in Liquid and Movement Analysis on NMG Plates. Standard thrashing assays were performed to compare the frequency of body muscle contractibility of WT and mutant animals. Individual young adult animals (24 h after L4) were transferred into a drop of 20 μL M9 buffer. After 1 min, the number of thrashes was recorded for 1 min and counted manually. A single thrash is defined as a complete sinusoidal movement through the head and tail.

For movement analysis on plates, 1- to 2-min videos of young adult stage animals crawling on the OP50-seeded NGM plates were recorded with a standard digital camera installed on a Leica MS5 dissecting microscope. Images were sampled from the videos at 1 frame per s and processed by in-house–developed ImageJ plug-ins. The longest distance of the outline of a detected object was calculated, and points giving this value were assigned as the head or tail positions. The anterior to posterior direction of the assigned points was manually determined and assigned in the first frame and tracked automatically by an in-house–developed plug-ins. The distance between the center points of the head-to-tail positions between two consecutive frames was calculated to determine the status of movement. The percentage of total frames exhibiting forward and backward movement at each pixel value was determined by using the pooled image frames from multiple animals of the same genotype.

Tissue-Specific Expression and Rescue of *egl-19(n582)*. *egl-19(n582)* mutants were injected with a DNA mix consisting of fosmid WRM0617aA03 (~2 ng/μl) that harbors the entire *egl-19* genomic region and an injection marker pTG95.62 (*sur-5::GFP*, ~15 ng/μl). Transgenic lines were selected by picking animals with bright nuclei-restricted GFP. Transgenic lines with a rescue of the sluggish locomotion, as well as defective egg-laying phenotypes exhibited by the *egl-19(n582)* mutants, were maintained to generate mosaic animals for both electrophysiology and locomotion analyses.

From the rescued transgenic Po parents, we screened for mosaic progenies that retained the transgene in either both neurons and muscles (N + M), or in neurons (N) by following GFP positive cells. Individual mosaic animals were then glued, dissected and recording, or subjected to thrashing and locomotion assays as described above.

For unknown reason, it was difficult to obtain *egl-19(n582)* mosaic animals expressing a WT EGL-19 transgene only in muscle cells (M). To generate a stable muscle EGL-19 transgene array, we isolated a 3.6-kb *egl-19* N-terminal partial cDNA fragment encoding amino acids 1–1197 of C48A7.1a by RT-PCR and cloned it into the BamHI/KpnI sites of a P*myo-3* promoter containing vector pJH580 to generate pJH2152. A 6.0-kb SalI/KpnI fragment that contains P*myo-3-egl*-19 partial cDNA fragment was purified from pJH2152 and coinjected with a fosmid WRM0620bD05, which overlaps with the last 477 bp of the Sal/KpnI fragment, along with a P*odr-1*-GFP injection marker in *egl-19(n582)* mutants. Transgenic lines were selected by picking animals with GFP-positive head sensory neurons by P*odr-1*-GFP. The proper recombination between the *Pmyo-3-egl-19* N-terminal cDNA, and the overlapping, "promoterless" *egl-19* genomic clone in transgenic lines were confirmed by PCR with a primer

pair that recognizes specifically the recombined minigene. These transgenic animals were then used for recordings and locomotion assays as described above.

Statistic Analysis. Two-tailed Student's *t* test was used to compare the difference of most datasets. $P < 0.05$ was considered statistically significant. Subsequent analysis and graphing were performed by using Excel (Microsoft), Igor Pro (Wavemetrics), and Clampfit (Molecular Devices). In this study, each cell recording is from one animal unless otherwise noted. For *egl-19(lf)*, *unc-36(lf)*, *shk-1(lf)*, and *slo-1(gf)* mutants, more than three action potentials per animal were analyzed and their mean was used as a data point for each animal, whereas more than five action potentials per animal were analyzed for WT and other mutant animals. Unless otherwise noted, data are presented as means ± SEM.

1. Brenner S (1974) The genetics of *Caenorhabditis elegans*. *Genetics* 77:71–94.
2. Liewald JF, et al. (2008) Optogenetic analysis of synaptic function. *Nat Methods* 5: 895–902.
3. Richmond JE, Jorgensen EM (1999) One GABA and two acetylcholine receptors function at the *C. elegans* neuromuscular junction. *Nat Neurosci* 2:791–797.

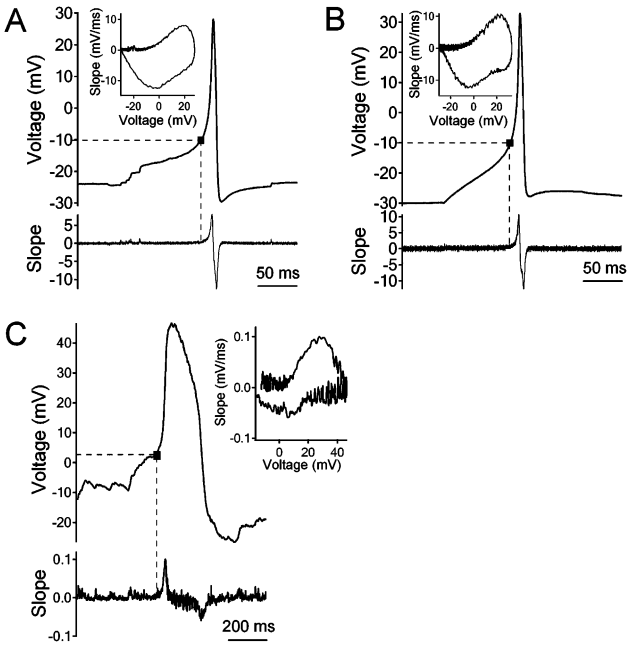

Fig. S1. Action potential threshold. (*A*) An example of spontaneous action potential by body wall muscles aligned with the derivative of action potential voltage (Slope). The action potential threshold was defined as the initial voltage after the rapid rise of action potential slope. *Inset* shows the voltage phase-plane projection (d*V*/d*t*) versus membrane potential. The dashed lines and square indicate the threshold value of the action potential. (*B*) An example of an action potential evoked by 10 pA current injection aligned with the derivative of action potential voltage (Slope). (*C*) The action potential in *egl-19(n582)* exhibited a higher threshold, which was defined and marked similarly as in *A* and *B*.

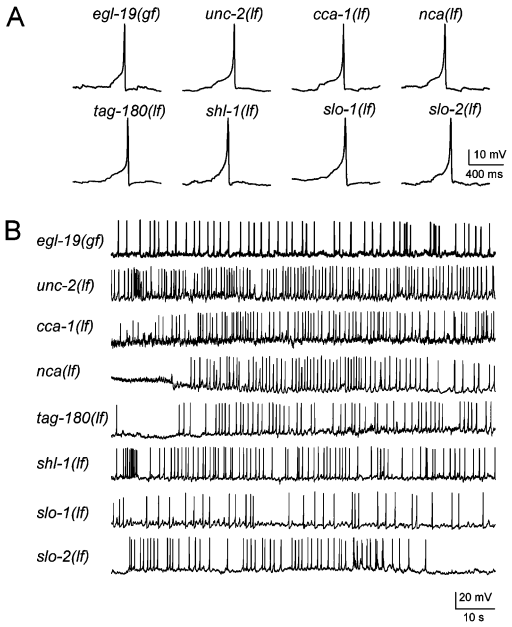

Fig. S2. The kinetics and frequency of action potentials in various channel mutants. (*A*) Representative traces for single action potentials in different mutant backgrounds. (*B*) Representative traces of spontaneous action potential trains in each mutant. Recordings were sustained for at least 100 s.

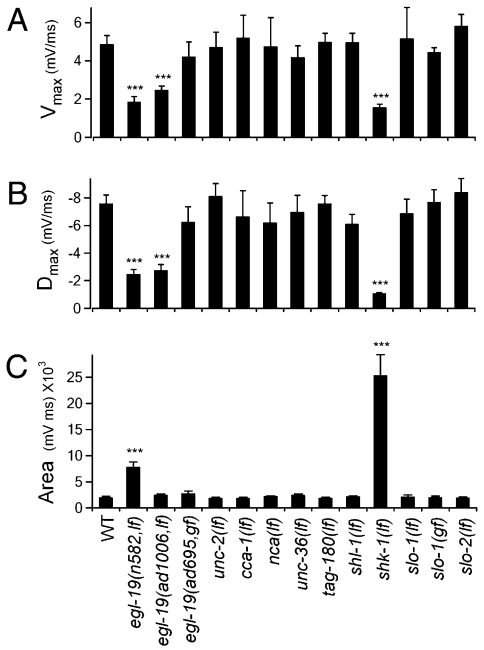

Fig. S3. Quantification of the kinetics of spontaneous action potentials in various channel mutants. (*A* and *B*) Maximum rising slope and decay slope (mV/ms) were significantly reduced in *egl-19(n582)*, *egl-19(ad1006)*, and *shk-1(lf)* mutants. (*C*) Action potential area (mV/ms) was significantly increased in *egl-19(n582)* and *shk-1(lf)* mutants. $^{**}P < 0.01$; $^{***}P < 0.001$; *t* test against WT. (Error bars = SEM.)

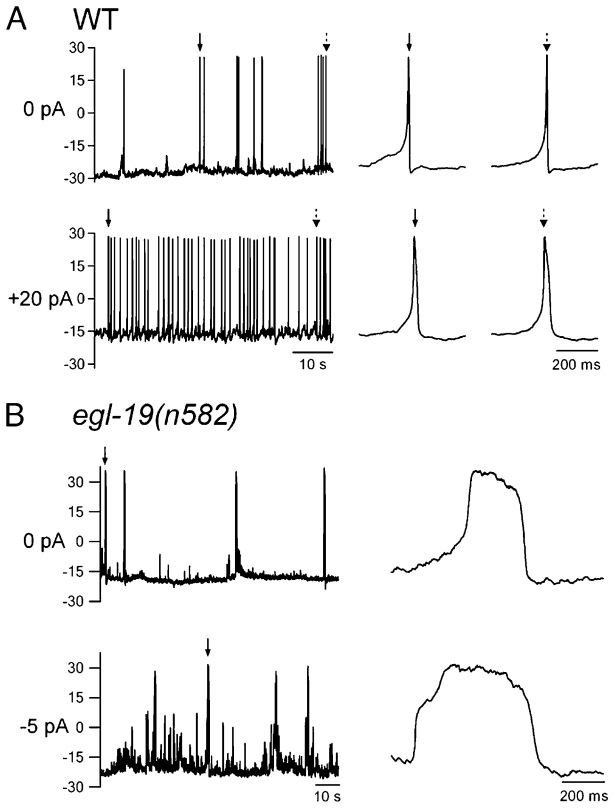

Fig. S4. Depolarizing resting membrane potential had a mild effect on action potential kinetics. (*A Upper*) Representative spontaneous action potentials firing pattern with the resting membrane potential at approximately −30 mV in WT. (*Lower*) The resting membrane potential was depolarized to −15 mV in the same muscle by +20-pA current injection. *Right* showed two single action potentials that exhibited a slightly prolonged duration and decreased amplitude at −15 mV. (*B Upper*) Representative traces of action potentials with the resting membrane potential at approximately −15 mV in *egl-19(n582)*. (*Lower*) The action potential kinetics was not restored when the membrane potential was hyperpolarized to approximately −25 mV by −5-pA current injection. *Right* showed single action potentials that exhibited a slightly prolonged duration at −25 mV.

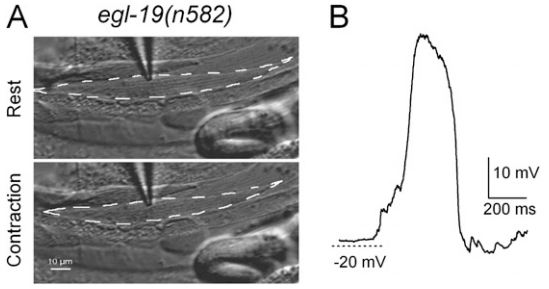

Fig. S5. Single spontaneous action potentials drove body wall muscle contractions in *egl-19(n582)* mutants. (*A*) Representative muscle morphology before (Rest) and during (Contraction) the action potential firing. (*B*) Action potentials were simultaneously recorded in the same muscle.

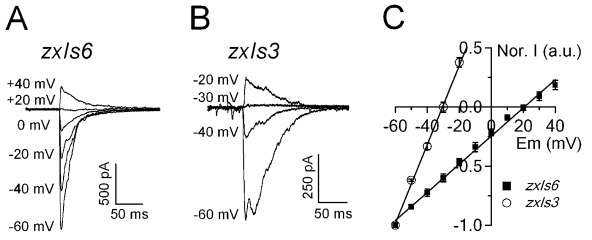

Fig. S6. Reversal potentials of ACh and GABA receptors in *C. elegans* body wall muscles. (*A*) Representative traces for currents evoked by 10-ms light stimulation at 30-s interval in *zxIs6* animals from −60 to +40 mV. (*B*) Representative traces for currents evoked by 10-ms light stimulation in *zxIs3* animals from −60 to −20 mV. (*C*) Normalized peak currents were plotted with different voltages in *zxIs6* and *zxIs3* animals. Linear fitting showed reversal potentials of +20 mV (n = 8) and −30 mV (n = 7) in *zxIs6* and *zxIs3*, respectively.

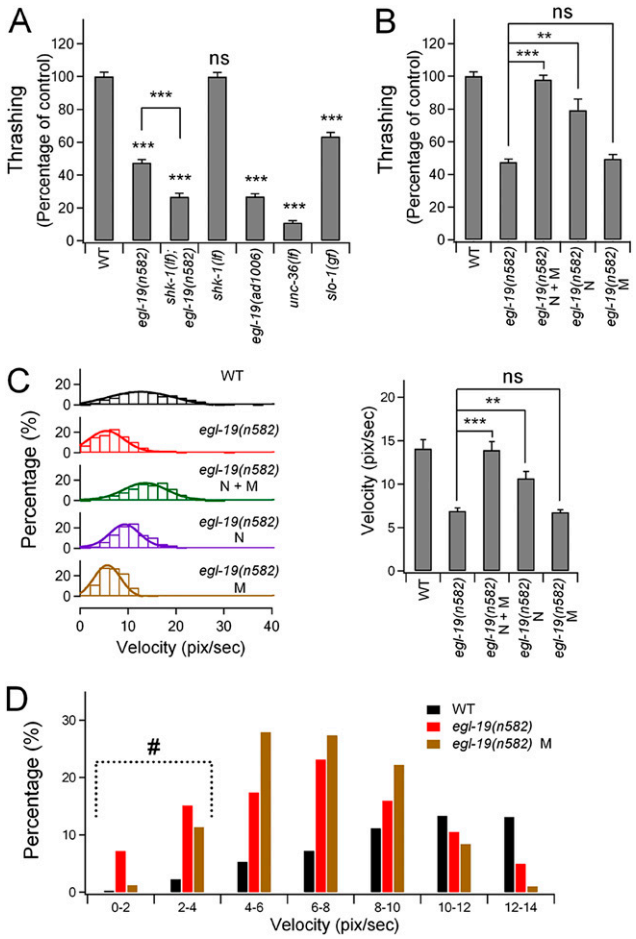

Fig. S7. Both neuronal and muscle EGL-19 expression are required to rescue the sluggishness movement of *egl-19(n582)* animals. (*A*) The frequency of body bending in M9 buffer in wild-type (WT) animals and mutants exhibiting defective action potential frequency and/or kinetics. All mutants (except *shk-1(lf)*) that affect action potential patterns showed a decreased thrashing frequency. *shk-1(lf);egl-19(n582)* double-mutant animals further enhanced the thrashing deficit of *egl-19(n582)* mutants. (n = 8 animals per genotype in each set of the thrashing assay, and the assay was repeated twice.) Asterisks denote the statistically significant difference against WT animals unless specified. (*B*) The reduced body-bending frequency of *egl-19(n582)* mutants was fully rescued in transgenic animals that expressed a functional EGL-19 transgene in both neurons and muscles (N + M), partially rescued when transgene was in neurons alone (N), and not rescued when expressed in muscles alone (M). (n = 8 animals per genotype in each set, and the experiment was repeated twice.) Asterisks represent statistically significant difference against *egl-19(n582)* animals. (*C*) The velocity of WT, *egl-19(n582)*, and *egl-19(n582)* N + M, *egl-19(n582)* N, and *egl-19(n582)* M animals on NGM plates seeded with OP50. (*Left*) The distribution (percentage of total video frames) of the speed (pixels per s) for animals of each genotype. (*Right*) The mean velocity of each genotype. The mean speed of *egl-19(n582)* N + M animals were restored to WT level, whereas *egl-19(n582)* N animals exhibited partial rescue, and *egl-19(n582)* M animals showed no statistically significant improvement in the mean velocity. (n = 360, 363, 403, 364, and 406 video frames collected from 10, 11, 11, 10, and 11 WT, *egl-19(n582)*, and *egl-19(n582)* N + M; *egl-19(n582)* N; and *egl-19(n582)* M animals, respectively. Asterisks represent statistical significance against *egl-19(n582)* animals. (*D*) *egl-19(n582)* M animals exhibited a slight improvement in speed compared with *egl-19(n582)* animals (#), although the improvement did not result in a statistically significant increase of the mean velocity. ns, not significant. $*P < 0.05$; $**P < 0.01$; $***P < 0.001$. (Error bars = SEM.)

Table S1. Summary of parameters of action potentials in different genotypes

Genotype	*n*	Channel type	Subunit	RMP, mV	Freq., Hz	Action potential kinetics					
						n	Amp., mV	Duration, ms	V_{max}, mV/ms	D_{max}, mV/ms	Area, mV/ms
WT	10			−24.5 ± 1.4	0.73 ± 0.14	8	46.0 ± 2.2	14.9 ± 1.2	4.9 ± 0.5	−7.6 ± 0.6	2,017.6 ± 184.2
egl-19(n582)IV	9	L-VGCC	α_1	−15.2 ± 1.4*	0.03 ± 0.01***	5	47.5 ± 1.3	152.1 ± 22.8**	1.9 ± 0.3***	−2.5 ± 0.4***	7,840.5 ± 949.2**
egl-19(ad1006)IV	7	L-VGCC	α_1	−25.9 ± 1.8	0.12 ± 0.03**	8	33.9 ± 2.1**	38.4 ± 5.0**	2.5 ± 0.2***	−2.8 ± 0.4***	2,464.0 ± 228.9
egl-19(ad695)IV gf	9	L-VGCC	α_1	−25.9 ± 2.6	0.75 ± 0.14	6	43.9 ± 2.9	17.8 ± 2.1	4.2 ± 0.8	−6.2 ± 1.1	2,802.2 ± 407.7
unc-2(e55)X	7	R,N,P/Q-VGCC	α_1	−23.9 ± 2.1	0.65 ± 0.10	4	45.1 ± 3.8	14.2 ± 1.5	4.7 ± 0.8	−8.1 ± 0.9	1,899.6 ± 180.2
cca-1(ad1650)X	5	T-VGCC	α_1	−23.8 ± 2.7	0.67 ± 0.13	5	44.8 ± 3.6	16.8 ± 3.0	5.2 ± 1.2	−6.6 ± 1.9	1,898.5 ± 150.3
nca-1(gk9)IV; nca-2(gk5)III	5	NALCN	α	−23.8 ± 1.0	0.78 ± 0.10	5	44.1 ± 4.1	19.8 ± 3.1	4.8 ± 1.5	−6.2 ± 1.4	2,283.2 ± 38.4
unc-36(e251)III	8	L-VGCC	$\alpha_2\delta$	−25.0 ± 2.6	0.07 ± 0.02***	6	45.5 ± 2.2	18.0 ± 2.2	4.2 ± 0.6	−7.0 ± 1.2	2,467.7 ± 197.6
tag-180(ok779)II	7	L-VGCC	$\alpha_2\delta$	−23.7 ± 2.4	0.71 ± 0.18	5	44.5 ± 1.9	14.8 ± 1.1	5.0 ± 0.5	−7.6 ± 0.6	1,892.4 ± 97.6
shl-1(ok1168)IV	6	Kv4	α	−24.8 ± 1.8	0.67 ± 0.17	8	45.3 ± 2.1	20.8 ± 2.4	5.0 ± 0.5	−6.1 ± 0.7	2,230.7 ± 110.8
shk-1(ok1581)II	15	Kv1	α	−25.1 ± 1.3	0.05 ± 0.01***	9	55.5 ± 2.2*	421.9 ± 35.8***	1.6 ± 0.2***	−1.1 ± 0.1***	25,319.8 ± 4,013.5***
slo-1(js379)V	8	BK	α	−24.3 ± 3.0	0.75 ± 0.11	3	45.9 ± 3.9	16.6 ± 4.3	5.2 ± 1.6	−6.9 ± 1.0	2,127.8 ± 343.3
slo-1(ky389)V gf	10	BK	α	−26.5 ± 2.5	0.05 ± 0.02***	6	44.2 ± 0.6	16.0 ± 1.5	4.4 ± 0.2	−7.7 ± 0.9	2,066.5 ± 187.6
slo-2(nf100)X	7	K_{Na}	α	−25.6 ± 1.7	0.76 ± 0.13	6	44.3 ± 1.6	14.4 ± 2.1	5.8 ± 0.6	−8.4 ± 1.0	1,966.6 ± 149.6

RMP, resting membrane potential; V_{max}, maximum upstroke slope; D_{max}, maximum decay slope; *gf*, gain-of-function [others are loss-of-function (*lf*) mutants]. *$P < 0.05$; **$P < 0.01$; ***$P < 0.001$; *t* test against WT. (All error bars = SEM.) Light gray shading, Ca^{2+} channels; dark gray shading, K^+ channels.

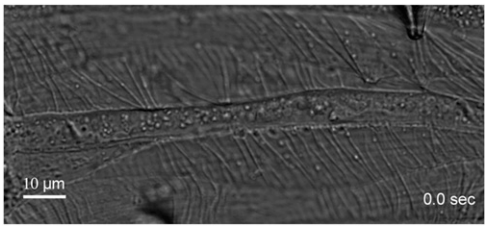

Movie S1. Muscle response in *zxIs6* (0.1 ms). A 0.1-ms light stimulation failed to induce obvious body wall muscle contractions in *zxIs6* animals.

Movie S1

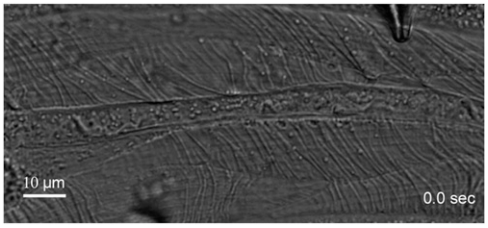

Movie S2. Muscle response in *zxIs6* (1 ms). A 1-ms light stimulation drove a brief body wall muscle contractions in *zxIs6* animals.

Movie S2

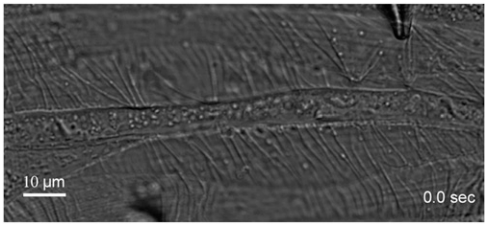

Movie S3. Muscle response in *zxIs6* (1 s). A 1-s light stimulation drove sustained body wall muscle contractions in *zxIs6* animals.

Movie S3

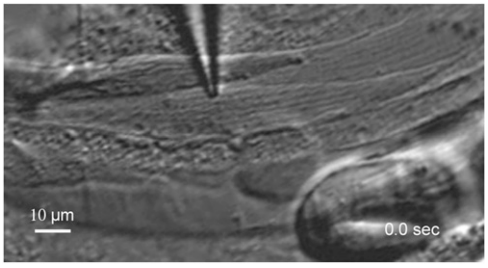

Movie S4. Muscle contraction in *egl-19(n582)*. Single spontaneous action potential drove body wall muscle contractions in *egl-19(n582)* animals.

Movie S4

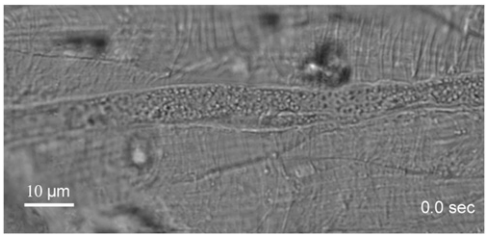

Movie S5. Muscle response in *zxIs3* (1 s). A 1-s light stimulation drove body wall muscle relaxation in *zxIs3* animals.

Movie S5